Transportation Safety and Environment, 2020, Vol. 2, No. 1 58–68

doi: 10.1093/tse/tdaa001
Research Article

RESEARCH ARTICLE

Effect of superabsorbent polymer on mechanical properties of cement stabilized base and its mechanism

Yongsheng Guan[1], Zhixiang Zhang[1], Xiaorui Zhang[2], Junqing Zhu[2,*], Wen Zhou[1], Qi Huang[1] and Yuqing Zhang[3,4]

[1] Jiangsu Sinoroad Engineering Research Institute Co. LTD, 99-196 Taizhong Rd, Nanjing 211805, China, [2]School of Transportation Engineering, Southeast University, #2 Sipailou, Nanjing 210096, China, [3]National Engineering Laboratory of Highway Maintenance Technology, Changsha University of Science & Technology, Changsha 410114, China and [4]Aston Institute of Materials Research, Engineering Systems & Management Group, Aston University, Birmingham, B4 7ET, UK

*Corresponding author. E-mail: zhujunqing@seu.edu.cn

Abstract

Superabsorbent polymers (SAPs) are cross-linked polymers that can absorb and retain large amounts of water. In recent years, a growing interest was seen in applying SAPs in concrete to improve its performance due to its efficiency in mitigating shrinkage. This paper presents findings in a study on effect of SAPs on performance of cement-treated base (CTB), using the experience of internal curing of concrete. CTB specimens with and without SAPs were prepared and tested in the laboratory. Tests conducted include mechanical property testing, dry shrinkage testing, differential thermal analysis, mercury intrusion porosimetry and scanning electron microscope testing. It was found that 7-day and 28-day unconfined compressive strength of CTB specimens with SAPs was higher than regular CTB specimens. 28d compressive strength of CTB specimens with SAPs made by Static pressure method was 5.87 MPa, which is 27% higher than that of regular CTB specimens. Drying shrinkage of CTB specimens with SAPs was decreased by 52.5% comparing with regular CTB specimens. Through the microstructure analysis it was found that CTB specimens with SAPs could produce more hydration products, which is also the reason for the strength improvement.

Keywords: superabsorbent polymer; cement-stabilized base; internal curing; mechanical property; drying shrinkage

Received: October 14, 2019. **Revised:** February 8, 2020. **Accepted:** March 12, 2020

1. Introduction

Semi-rigid base asphalt pavement is one of the most commonly used highway pavement structures in many countries. Cement-stabilized gravel is widely used as semi-rigid base due to its high strength, good stability and strong integrity. However, there are still many problems in the application of cement stabilized gravel in pavement structure such as moisture damage and cracking [1, 2, 3].

High-performance concrete (HPC) has been widely used as building construction material. It contains an excess amount of Portland cement relative to free water (low water–cement ratio), which results in a phenomenon known as 'self-desiccation' [4]. As cement reacts with water, hydration products will precipitate in the water-filled spaces between the solid particles in the cementitious material [5]. The water in the remaining small capillaries forms menisci and exerts hydrostatic tension forces. These capillary forces reduce the distance between the solid particles, leading to autogenous shrinkage [6, 7]. In HPC mixes, significant inward Laplace pressures will develop as the water is consumed and drained from the smallest pores within the hydrated cement network. These pressures are high enough to cause a bulk volumetric collapse of the system referred to as autogenous shrinkage, which can result in early-age cracking and structural failure, especially if the concrete is restrained against forms, reinforcements, or other concrete [8, 9].

Internal curing has been proven effective in alleviating autogenous shrinkage cracking in HPC. The use of superabsorbent polymers (SAPs) in cementitious materials has seen an increased interest in the past decade due to its efficiency in mitigating autogenous shrinkage [10, 11]. Studies have shown that the concrete microstructure must be sufficiently permeable to allow any retained water within the hydrogel to refill as many voids as possible and aid in hydration, without increasing capillary porosity. Also, microstructural properties directly affect the strength of the cementitious material [12]. The amount of retained water in hydrogels governs the size of voids in the microstructure and thus plays an important role in mechanical properties [13, 14].

Methods for improving cracking resistance of semi-rigid base include adding a crack-resistant geogrid layer, pre-cracking the base layer and optimizing material performance by adding certain polymers with better cracking resistance in the mixture [15–19]. These polymers mainly consist of fibres and resins. Researchers have applied SAP as an internal curing agent in Portland cement concrete (PCC), which could greatly reduce the self-shrinkage of PCC and prevent early cracking. Also, improved impermeability, low-temperature cracking resistance, and workability was found by adding SAP [20–24]. Dang *et al.* [25] found that the incorporation of pre-absorbed SAP in concrete has a significant effect on the early self-shrinkage of high-strength concrete [26, 27]. Kim et al. used the non-metallic mineral polymer water-absorbent composite material to internally maintain the concrete, which greatly improved the self-shrinkage and drying shrinkage of the concrete and improved its cracking resistance [28, 29]. Lura *et al.* [30] and Zhu *et al.* [31] concluded that SAP could significantly reduce the plastic shrinkage of concrete, and particle size of SAP has a certain influence on the curing effect. The effect of reducing plastic shrinkage increases with particle size, and ∼50% decrease can be observed in the reference concrete at its maximum effect [32].

In this study, SAPs were prepared and used as a novel self-curing admixture in cement-treated base (CTB). The objective of this study is to evaluate the effect of SAP on performance of CTB. It is expected to store water in the early stage and release the moisture in the later stage for the internal curing of concrete mixture, which solves the problem of the hydration in pavement structure in the high-temperature season.

2. Materials and methods

2.1. Raw material properties

2.1.1. *Cement.* P.O. 42.5 retarding cement is used in this study. Strength specimens are formed according to the normal consistency method. Physical properties of the cement are shown in Table 1.

2.1.2. *Superabsorbent polymer.* SAP materials are hydrophilic networks that can absorb and retain huge amounts of water or aqueous solutions [33]. Basic physical properties of SAP used in this study are presented in Table 2. Appearance of SAP before water absorption is white powder as shown in Fig. 1a and is gel-like after water absorption as shown in Fig. 1b.

2.1.3. *Aggregate.* Clean crushed gravel was used as aggregate and was well graded based on the specified sizes. The specified aggregate size is 9.5–31.5 mm, 4.75–9.5 mm, 2.36–4.75 mm and 0–2.36 mm, named by four different numbers from No.1 to No.4. Aggregate were selected complying

Table 1. Physical properties of cement

Item	Water requirement for normal consistency (%)	Soundness (mm)	Setting time (min)		Bending strength (MPa)		Compressive strength (MPa)	
			Initial	Final	3d	7d	3d	7d
Cement	27.6	1.0	312	378	5.0	7.6	24.9	46.3
Specifications	—	≤5.0	≥180	≥360	≥3.5	≥6.5	≥17.0	≥42.5

Table 2. Performance tests of SAP

Item	Unit	Result
PH value	–	6.3
Particle size distribution		
>150 μm	%	37.6
106–150 μm	%	60.5
75–106 μm	%	1.9
<75 μm	%	0
Density	g/cm^3	0.64
Absorption rate (physiological saline)	S	15
Saline absorption	g/g	52
Moisture holding capacity	g/g	28
Absorption with load	g/g	17
Distilled water absorption	g/g	360
Tap water absorption	g/g	210.8

(a) (b)

Fig. 1. SAP in different appearances: (a) before water absorption; (b) after water absorption

with recommendations as follows: (1) crushing value of crushed stone in all aggregate should be ≤28% and needle-like content of coarse aggregate should be no more than 18% (preferably ≤15%); (2) passing rate of 0.075 mm in material No. 4 should be ≤20% (preferably ≤18%); (3) aggregate with size < 0.6 mm in the gravel must be tested for liquid limit and plasticity index, which requires a liquid limit < 28% and the plasticity index < 9. Fig. 2 and Table 3 present the gradation of crushed gravel.

2.2. Mix design

The dosage of SAP and additional water are determined according to the orthogonal test method as shown in Tables 4–6. Influence of each level of single factor on the test results was analysed by the size of k value, and the main and secondary effects

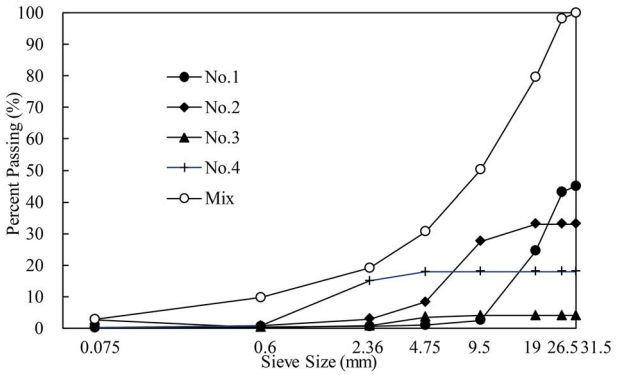

Fig. 2. Gradation of aggregate and mix

of each factor were judged by the size of R [34]. According to the data comparison in Tables 4–6, the optimal level of each factor is SAP of Class a, 1% of the superabsorbent resin, and 10 times of additional water. According to the R value of range, the main order of the impact on compressive strength is additional water amount > superabsorbent resin content > superabsorbent resin type.

It was determined that the amount of SAP is 1% of the amount of cement, and the amount of additional water is 10 times of SAP mass. Because of the existing additional water, the optimal moisture content is required between 4.5 and 5.5% to process the mixture design. The optimal moisture content and maximum dry density is determined from peak points on the dry density—moisture content curve. Standard test method JTG E51–2009 was followed in the process [35]. Both vibration compaction and impact compaction methods were used. The design results of the mixture ratio are shown in Table 7.

The cement-stabilized gravel mixture design process mainly includes two compaction methods, which are static pressure compaction method and vibration compaction method. Testing parameters include dry density, water content and strength.

2.3. Testing plan

Dry shrinkage test, unconfined compressive strength test and the split test of the CTB specimens were carried out in accordance with standard test

Table 3. Gradation of cement stabilized gravel (passing%)

Aggregate	Proportion (%)	Sieve size (mm)							
		31.5	26.5	19.0	9.5	4.75	2.36	0.6	0.075
No.1	45.0	45.0	43.1	24.5	2.5	0.9	0.5	0.4	0.1
No.2	33.0	33.0	33.0	33.0	27.5	8.3	2.9	0.7	0.1
No.3	4.0	4.0	4.0	4.0	4.0	3.5	0.7	0.2	2.6
No.4	18.0	18.0	18.0	18.0	18.0	17.9	15.0	0.7	0.1
Mixture gradation		100	98.1	79.5	50.2	30.6	19.1	9.7	2.8

Table 4. Factor level

Level	A SAP resin type	B SAP resin content	C Additional water amount
1	a	0.6%	10
2	b	0.8%	20
3	c	1.0%	30

Table 5. Orthogonal test scheme and results

#	A	B	C	3d unconfined compressive strength/MPa	7d unconfined compressive strength/MPa
1	1	1	1	10.41	10.62
2	1	2	2	10.88	11.05
3	1	3	3	10.22	10.39
4	2	1	2	9.64	9.89
5	2	2	3	9.94	10.06
6	2	3	1	10.87	10.99
7	3	1	3	9.93	10.12
8	3	2	1	10.36	10.51
9	3	3	2	10.58	10.73

Table 6. 7d strength range analysis of specimens

Group number	A	B	C
K1	32.06	30.63	32.12
K2	30.94	31.62	31.67
K3	31.36	32.11	30.57
k1	10.69	10.21	10.71
k2	10.31	10.54	10.56
k3	10.45	10.70	10.19
Range R	0.24	0.49	0.52
Factors in the order	Additional water amount	SAP resin content	SAP resin type
Optimal levels	A	1.0%	10

methods in 'Test Methods of Materials Stabilized with Inorganic Binders for Highway Engineering' (JTG E51–2009) [35]. The microscopic test samples, which did not contain aggregates, were taken from the cement slurry in the CTB specimen. A brief introduction of each test is presented in following sections.

2.3.1. Dry shrinkage test. Standard test method T0854–2009 was followed in conducting this test [35, 36]. Four specimens of the same mix proportion were used for testing. Two specimens were used to measure the shrinkage and deformation of the materials. The other two specimens were reserved for measuring the water loss rate in dry shrinkage of the materials. Temperature was maintained at ~20°C. The middle beam that has been soaked for a day is taken out of the water, and the surface moisture of the specimen is absorbed with a soft cloth. The initial length of the specimen used to measure the contraction deformation is measured with a Vernier caliper, and the initial mass of the specimen used to measure the water loss rate. First, a dial gauge is installed on the shrink metre and a glass rod with lubricant is placed. Then, the long shaft end of the specimen used to measure the contraction deformation is ground and attached to the organic glass sheet. After the glue has set, the middle beam specimen is put on

Table 7. Design result of mixture proportion in cement stabilized gravel

Aggregate Percentage (%)				Cement dosage (%)	Maximum dry density (g/cm^3)		Optimal moisture content (%)		Designed strength (MPa)
No.1	No.2	No.3	No.4		Vibration	Impact	Vibration	Impact	
45.0	33.0	4.0	18.0	4.5	2.456	2.390	4.8	5.0	4.3

the shrink metre and the test begins. At the start of test within a week, read the data once a day, write down the reading of four dial gauge used to measure shrinkage strain of specimen, weigh the specimen that is used to measure the quality of the water loss rate. After 7 days, read the data every 2 days until a month. Dry the specimen that will be used to measure the water loss rate to the constant weight and weigh its mass.

If the drying shrinkage strain of the two adjacent measuring points at a certain temperature is ε_i, ε_{i+1}, and the water content of the mixture is ω_i and ω_{i+1}, then the average dry shrinkage coefficient of this section is:

$$\alpha_d = \frac{\varepsilon_{i+1} - \varepsilon_i}{\omega_{i+1} - \omega_i}, \quad (1)$$

where, ω_i, ω_{i+1}—the moisture content of specimens measured at two adjacent measuring points; ε_i, ε_{i+1}—the dry shrinkage strain values of two adjacent specimens.

2.3.2. Unconfined compressive strength test. Standard test method T0805–1994 was followed in conducting this test [35]. Based on the type of test materials and general engineering experience, the failure load of the specimens should be >20% of the measured force range and <80% of the measured force range when the dynamometer and press machine with appropriate range are selected. Oil is applied to the spherical support and upper and lower roof, enabling the spherical support to rotate flexibly.

The test specimen that has been soaked for 1 day is taken out of the water, and the surface moisture of the test piece is absorbed with soft cloth. Then, the test specimen is put on the pavement material strength tester or pressure machine, and a flat ball seat is placed on the lifting table for the compression test. During the test, the loading rate should be kept at 1 mm/min. The maximum pressure at failure is recorded. The unconfined compressive strength of the specimen is calculated as follows:

$$R_c = \frac{P}{A}, \quad (2)$$

where R_c is unconfined compressive strength (MPa) of the specimen; P is the maximum pressure (N) at failure of specimens; and A is the cross-sectional area of the specimen (mm^2).

2.3.3. Splitting tensile strength test. Standard test method T0806–1994 was followed in conducting this test [35]. Based on the type of test materials and general engineering experience, the failure load of the specimens should be more than 20% of the measured force range and <80% of the measured force range when the dynamometer and press machine with appropriate range are selected. Oil is applied to the spherical support and upper and lower roof, enabling the spherical support to rotate flexibly. During the test, the deformation of the test should be increased at an equal rate, and the loading rate should be kept at 1 mm/min. The maximum pressure P_N at failure is recorded. The fracture tensile strength of the specimen is calculated as follows:

$$R_i = 2P/\pi dh\left(\sin 2\alpha\text{-}a/d\right), \quad (3)$$

where R_i is the indirect tensile strength (MPa) of the specimen; d is diameter of the specimen (mm); a is width of the tie bar (mm); α is the central angle corresponding to the width of semi-bar; P is the maximum pressure (N) of specimens at failure; and h is height of specimen (mm) after immersion.

2.3.4. Differential thermal analysis (DTA). DTA is a thermoanalytic technique that is similar to differential scanning calorimetry [DSC, 36]. The specimens are made to undergo identical thermal cycles, while recording any temperature difference between sample and reference. Thermogravimetric (TG) analysis and DSC analysis were conducted together with the test and are plotted against the temperature. TG measures weight changes in the specimen as a function of temperature. The DSC measures the difference in the amount of heat required to increase the temperature of the specimen and reference is measured as a function of temperature.

Table 8. Unconfined compressive strength test results

Compaction method	Category	Unconfined compressive strength (MPa)	
		7d	28d
Static pressure	CTB	3.94	4.62
	CTB w/SAP	4.47	5.87
	Strength growth rate/%	13.45	27.06
	Standard errors	0.38	0.88
Vibration	CTB	9.96	10.5
	CTB w/SAP	10.88	10.98
	Strength growth rate/%	9.24	4.57
	Standard errors	0.65	0.34

2.3.5. Mercury intrusion porosimetry (MIP). MIP is a technique that determines the percentage of open pores between 0.006 and 360 μm, together with the pore entrance size distribution, and also gives information on pore shape and tortuosity [37].

2.3.6. Scanning electronic microscopy (SEM). The principle of SEM is based on the interaction between electrons and matter [38, 39]. When scanning the sample surface with a beam of high-energy electrons, secondary electrons will be excited from the sample surface when the surface is scanned with a beam of high-energy electrons. The number of secondary electrons is related to the incident angle of the electron beam, so it is related to the surface structure of the sample. The secondary electrons are collected by the detector and transformed into electrical signals which form an image reflecting the surface characteristics of the sample. The secondary electronic signals are used in this SEM test.

3. Results and discussion

3.1. Mechanical properties

To evaluate the effect of SAP on the mechanical properties of CTB, mechanical properties of specimens prepared with static pressure compaction method and vibration compaction method were examined. Regular CTB and CTB with SAP were both prepared and tested. Table 8 presents the unconfined compressive strength test results of 7d and 28d and splitting tensile test results of 7d.

3.1.1. Unconfined compressive strength. It can be seen from Table 8 that 7d and 28d unconfined compressive strength of CTB specimens with SAP are higher than regular CTB specimens with both compaction methods. It indicates that adding SAP in mixture can significantly improve the early and long-term compressive strength of CTB. Volume of SAP became larger and formed gel after water absorption, which played a lubricating role between cement particles and aggregates. It could partly improve the workability of the binder and densify the internal structure. However, in the process of water loss, void will be left inside the specimen, increasing porosity of the specimen, but most of the increase is the harmless pores (pore diameter < 50 nm). The strength of the CTB specimens is mostly derived from the tight intercalation between aggregates under external pressure. Moreover, the addition of SAP made cement hydration more sufficient and pore diameter more refined. Thus, the compressive strength of the samples was increased.

Comparing the two compaction methods, the strength of the specimen prepared with static pressure compaction method is significantly lower than vibration method. Specimens prepared with vibration compaction method have higher compaction degree and thus have higher compressive strength. However, strength growth rate of specimens prepared with static pressure compaction method is relatively higher than vibration compaction method. The addition of SAP improved the workability of the binder and made the specimen more compacted. In addition, it increased the degree of cement hydration and increased the compressive strength of the specimen to some extent. For vibration compacted specimens, due to their higher overall compaction degree and smaller room for strength improvement, strength growth with addition of SAP is not as obvious as that of static pressure compacted specimens.

3.1.2. Splitting tensile strength. It can be seen from Table 9 that splitting tensile strength of the CTB specimens with SAP reached 0.41 MPa, comparing with 0.35 MPa of regular CTB specimens. It can be concluded that the addition of SAP material is beneficial to improve the cracking resistance of CTB. This is mainly due to SAP expanding

Table 9. Splitting tensile strength test results

Category	Splitting strength of 7d/MPa
CTB	0.35
CTB w/SAP	0.41
Strength growth rate/%	14.28

into gel after water absorption, which is between the cement particles and the aggregate and can partially improve the workability of the binder and can also densify the internal structure.

The strength of the CTB specimen comes from the close intercalation between the aggregates under external pressure, and the cement slurry only plays the role of filling and cementing in the mixture. In cement concrete, the addition of SAP will reduce the early strength of the specimen to some extent. This is because the formation of concrete strength mainly depends on the hydration of cement. When SAP is added to concrete mix, it can absorb a certain amount of water, which will reduce the moisture content inside the concrete and affect the early hydration of cement. With the increase of curing time, the water retained in SAP is gradually released, which promotes the later hydration of cement. Therefore, the addition of SAP will only reduce the early strength of cement concrete, and the impact on its later strength is limited. Because of the difference in strength forming between cement concrete and CTB, the water-stable base layer added to SAP present better composition and mechanical properties than that in ordinary water-stable base layer.

3.2. Dry shrinkage

The dry shrinkage strain of CTB specimen with and without SAP were compared as shown in Fig. 3.

As shown in Fig. 3, the addition of SAP could significantly reduce the drying shrinkage of CTB specimen. Dry shrinkage strain at 28d is 0.0183%, which is reduced by 52.5% from 0.0385% of the regular CTB specimen. Overall structure of the CTB specimen with SAP is denser than the regular CTB specimen, so the influence of chemical shrinkage caused by the continuous hydration of the cement is greatly reduced. On the other hand, the SAP has the characteristic of water retention. When the specimen loses water and its relative moisture content becomes small, the moisture stored before is released, so that the relative moisture content is appropriately replenished, which prevents or delays the shrinkage of the CTB

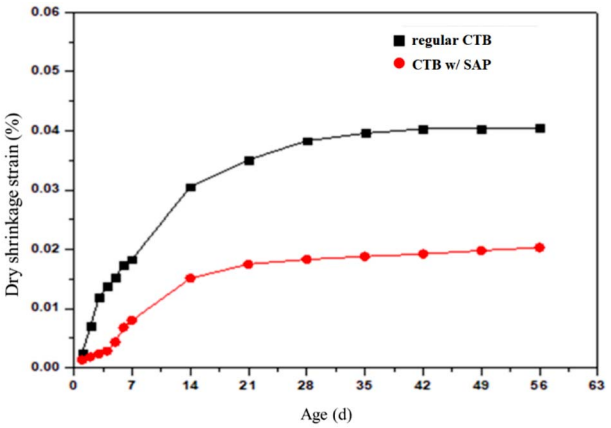

Fig. 3. Dry shrinkage strain curve of SAP and ordinary sample

Table 10. Weight loss in different temperature ranges

Item	Weight loss		
	20–200°C	200–1000°C	Total
CTB	8.07%	11.09%	19.16%
CTB w/SAP	5.98%	15.11%	21.09%

due to the increase of tensile strength. Therefore, dry shrinkage value of CTB specimen tends to be stable in the later stage, while dry shrinkage of regular CTB specimen still shows a slowly rising trend.

3.3. Micro-property analysis

3.3.1. Differential thermal analysis. Fig. 4 and Table 10 present the results of DTA of CTB specimens with and without SAP. The interval of temperature range was separated into lower than and >200°C to eliminate the effect of moisture absorbed by SAP on mass loss [40]. In the temperature range of 20–200°C, weight loss of CTB specimen with SAP is less than regular CTB specimen. In the temperature range of 200–1000°C, the weight loss of CTB specimen with SAP is larger than regular CTB specimen.

When the temperature rises to 200°C, the weight loss of the regular CTB specimen is 8.07%, and weight loss of CTB specimen with SAP is 5.98%. As shown in Fig. 4, an obvious endothermic peak accompanied by a certain weight loss appeared near 435°C. The appearance of this endothermic peak represents the dehydration decomposition of calcium hydroxide which is one of the main products of cement hydration. The weight loss of regular CTB specimen is 1.71%, and the weight loss of CTB specimen with SAP is 1.88%. In addition, the appearance of an endothermic peak ~682°C and 724°C are indicative of the further dehydra-

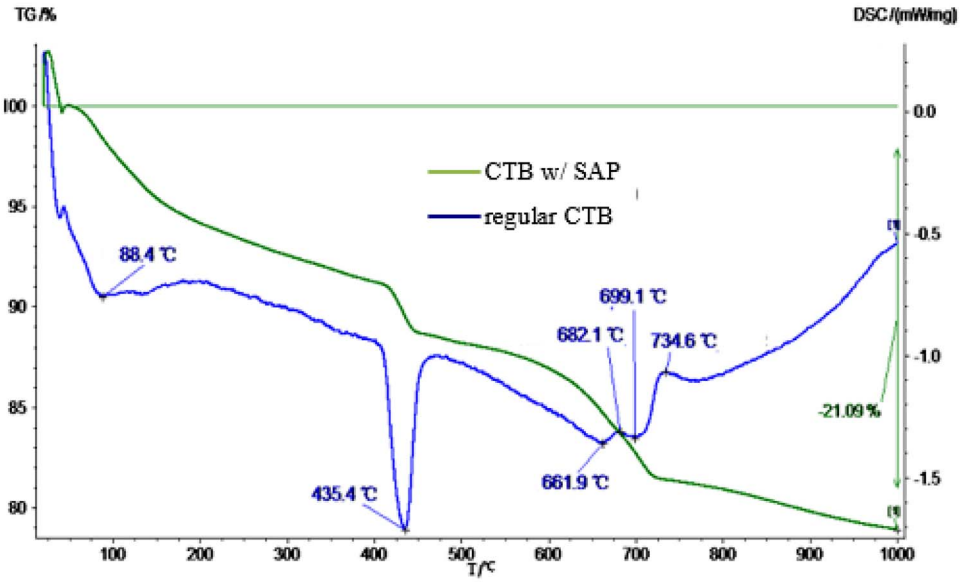

Fig. 4. Results of DTA

tion decomposition of the hydrated calcium silicate and the transition of the calcium silicate. In the CTB specimen with SAP, a slight exothermic peak appeared at around 660°C but there was no weight change, which was the decomposition of SAP under high-temperature conditions. It shows that the cement hydration in the CTB specimen with SAP is more complete, and more hydration products are formed, which is more conducive to the improvement of the strength of the CTB.

3.3.2. Structural analysis of mercury pore. The pore structure of the hardened cement slurry of the two sets CTB specimens were observed as shown in Table 11. Porosity indicates percentage using the volume of pores divided by the total volume of the sample; the median pore diameter is the corresponding pore diameter at 50% of the distribution of the pore diameter. The average pore diameter is four times volume of pores divided by the surface area of the pore based on the columnar model. The porosity of the cement slurry is increased after the addition of SAP as shown in Table 11, and the pores with diameter larger than 200 nm are more than the pore quantity of ordinary water stability sample. This is because the SAP gel will remain the space where pores in the cement slurry appear after dehydration. The larger voids make the porosity and average pore size of the CTB specimen with SAP larger than that in the regular CTB specimen.

The freeze-thaw damage of concrete is closely related to its internal microporous structure according to the theory of pore structure [41]. The pore can be divided into four grades according to the following sizes: $r < 20$ nm is harmless pore, $r = 20$–50 nm represents little harmful pore, $r = 50$–200 nm indicates medium harmful pore and $r > 200$ nm means highly harmful pore. The addition of SAP material in specimen can make the cement hydrate more complete, refine the pore size, and make the cement structure denser, so the proportion of tiny pores is higher than that in the regular CTB specimen.

The results in Table 11 reflect that the pore ratio of the CTB specimen with SAP with pore size < 50 nm (harmful and less harmful porn) is 59.5%, which is higher than 54.1% in the regular CTB specimen. In addition, the number of harmless pores in the SAP sample is more than in the ordinary sample. Although the ratio of macrospores in SAP sample is higher than in ordinary samples, the mechanical properties are better because the proportion of micropores is larger, cement is more hydrated and the structure is more compacted.

3.3.3. Scanning electron microscope. Fig. 5 demonstrate SEM images of CTB specimen with and without SAP at different ages. It is apparent from this figure that some typical cement hydration product such as C-S-H gel, ettringite or calcium hydroxide has been formed after the sample is moulded for 3 days [42, 43]. The hydration product produced by the CTB specimen with SAP is slightly more than the regular CTB specimen due to the addition

Table 11. Pore structure of each specimen

	Porosity (%)	Pore size (nm)		Pore size distribution			
		Median	Average	<20 nm	20–50 nm	50–200 nm	>200 nm
CTB	27.83	46.3	19.3	18.5	35.6	39.8	6.1
CTB w/SAP	30.87	37.9	21.9	23.8	35.7	29.3	11.2

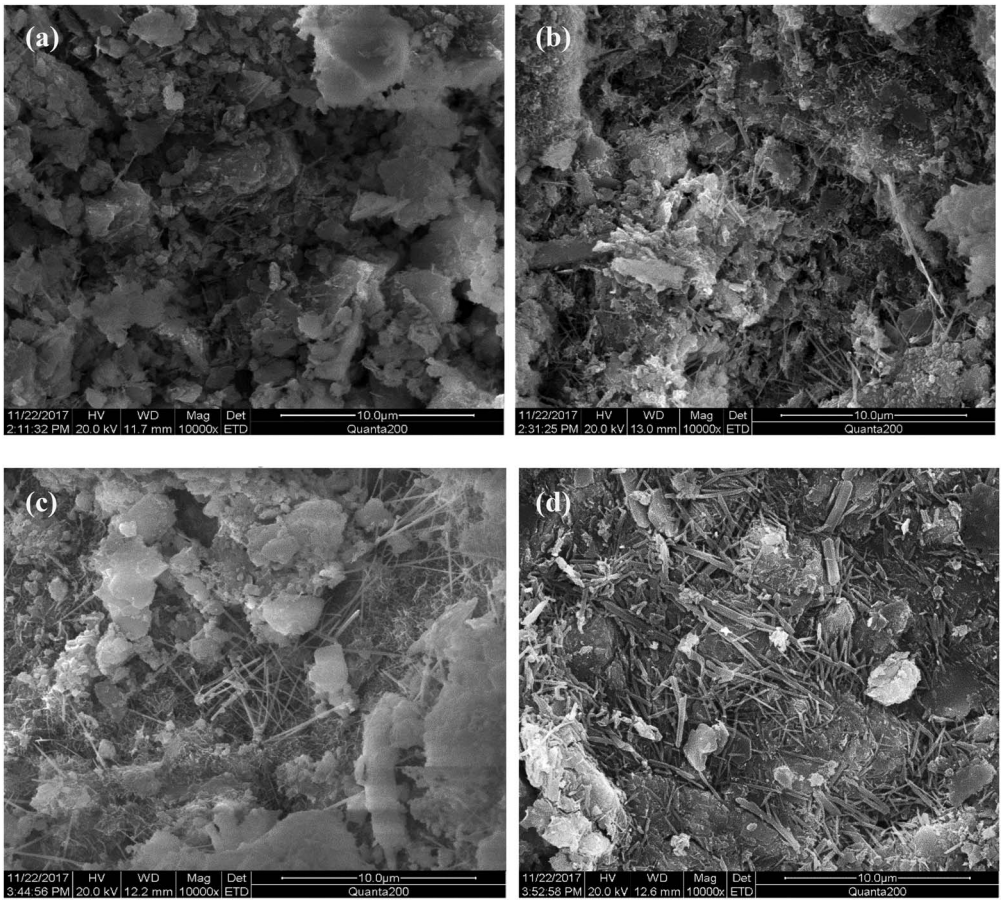

Fig. 5. SEM diagram of sample in each age: (a) regular CTB at 3rd; (b) CTB w/ SAP at 3rd; (c) regular CTB at 28d; (d) CTB w/ SAP at 28d

of additional water to the SAP sample. Besides, SAP material absorbs a certain amount of moisture, and the cement can be fully hydrated to produce more hydration product. In the later stage, the SAP sample will maintain a uniform and stable humidity inside, which is conducive to further hydration of the cement. In contrast, the moisture required for ordinary hydration of regular CTB specimen mainly comes from the external environment. Because the ambient humidity indoor is low, so its hydration speed is slower than that in CTB specimen with SAP. In the case of the same age, the hydration product produced by regular CTB specimen is less than CTB specimen with SAP, and regarding the macroscopic performance, the mechanical properties of CTB specimen with SAP are better than that in the regular CTB specimen.

4. Conclusions

SAP has an obvious effect on improving performance of CTB and is worth promotion. CTB specimens with and without SAP were prepared and tested in the laboratory. Orthogonal test method was used to determine the dosage of SAP and additional water content and the results indicated that the optimal level of each factor is SAP of Class a, 1% of the superabsorbent resin, and 10 times of additional water. Tests conducted include mechanical property testing, dry shrinkage

testing, DTA, mercury intrusion porosimetry and SEM testing. The following conclusions were drawn from this study.

(1) Effect of SAP on CTB was studied by different compaction methods. The unconfined compressive strength and splitting strength of CTB specimens with SAP were higher than regular CTB specimens, indicating adding SAP into CTB specimen can significantly improve its early and long-term compressive strength.

(2) The addition of SAP can effectively reduce the drying shrinkage of the CTB. Because the structure of the CTB specimen with SAP is relatively denser, the early shrinkage value of the specimen is significantly lower than regular CTB specimen, and the curve of dry shrinkage development in later stage is more inclined smooth. Compared to regular CTB specimen, its dry shrinkage value is reduced by 52.5%, which presents good crack resistance of the specimen with SAP material.

(3) Based on results of microscopic, it was found that the addition of SAP increased the proportion of harmless pores and less harmful pores. Although the proportion of harmful atmospheric pores was slightly increased, the pore structure was refined, and aperture distribution were also optimized. CTB specimen with SAP can produce more hydration products than regular CTB specimen in the early stage, resulting better mechanical properties.

Acknowledgements

This research was funded by the International Cooperation Project of Jiangsu Science and Technology Department [Grant No. BZ2017011].

Conflict of interest statement. The authors have declared that no conflict of interest exists.

References

1. Cusson D, Mechtcherine V, Lura P. Practical applications of superabsorbent polymers in concrete and other building materials. In: *Application of Super Absorbent Polymers (SAP) in Concrete Construction*. Netherlands: Springer, 2012, 137–48.
2. Farzanian K, Ghahremaninezhad A. On the effect of chemical composition on the desorption of superabsorbent hydrogels in contact with a porous cementitious material. *Gels* 2018a; **4**(3): 70.
3. Reinhardt HW, Assmann A, Mönnig S. Superabsorbent polymers (SAPs)-an admixture to increase the durability of concrete. *Proceedings of 1st International Conference on Microstructure Related Durability of Cementitious Composites*, Nanjing, China, October 13–15 2008; **10**: 313–323.
4. Zhu J, Ma T, Dong Z. Evaluation of optimum mixing conditions for rubberized asphalt mixture containing reclaimed asphalt pavement. *Construct Build Mater* 2020a; **234**:117426. https://doi.org/10.1016/j.conbuildmat.2019.117426.
5. Ding X, Ma T, Gu L, et al. Investigation of surface micro-crack growth behavior of asphalt mortar based on the designed innovative mesoscopic test. *Mater Design* 2019a; **185**:108238. https://doi.org/10.1016/j.matdes.2019.108238.
6. Ding X, Ma T, Gu L, et al. Discrete element methods for characterizing the elastic behavior of the granular particles. *J Testing and Evaluation* 2020; **48**:20190178. https://doi.org/10.1520/JTE20190178.
7. Snoeck D, Jensen OM, De Belie N. The influence of superabsorbent polymers on the autogenous shrinkage properties of cement pastes with supplementary cementitious materials. *Cem Concr Res* 2015; **74**:59–67.
8. Ding X, Ma T, Zhang W, et al. Experimental study of stable crumb rubber asphalt and asphalt mixture. *Construct Build Mater* 2017; **157**:975–81.
9. Krafcik MJ, Macke ND, Erk KA. Improved concrete materials with hydrogel-based internal curing agents. *Gels* 2017; **3**(4): 46.
10. Krafcik MJ, Erk KA. Characterization of superabsorbent poly (sodium-acrylate acrylamide) hydrogels and influence of chemical structure on internally cured mortar. *Mater Struct* 2016; **49**(11): 4765–4778.
11. Tang F, Zhu S, Xu G, et al. Influence by chemical constitution of aggregates on demulsification speed of emulsified asphalt based on UV-spectral analysis. *Construct Build Mater* 2019; **212**:102–8.
12. Snoeck D, Schaubroeck D, Dubruel P, et al. Effect of high amounts of superabsorbent polymers and additional water on the workability, microstructure and strength of mortars with a water-to-cement ratio of 0.50. *Construct Build Mater* 2014; **72**:148–57.
13. Farzanian F, Ghahremaninezhad A. Desorption of superabsorbent hydrogels with varied chemical compositions in cementitious materials. *Mater Struct* 2018b; **51**(1): 3.
14. Zhang T, Ma T, Ling M et al. Mechanistic sieve-size classification of aggregate gradation by characterizing load-carrying capacity of inner structures. *J Eng Mech* 2019a; **145**(9): 04019069-1-10. https://doi.org/10.1061/(ASCE)EM.1943-7889.0001640.
15. Hossain KMA, Ahmed S, Lachemi M. Lightweight concrete incorporating pumice based blended cement and aggregate: mechanical and durability characteristics. *Construct Build Mater* 2011; **25**(3): 1186–1195.
16. Kodikara J, Chakrabarti S. Modeling of moisture diffusion in crushed basaltic rock stabilized with cementitious binders. *J Mater Civ Eng* 2005; **17**(6): 703–710.
17. Kovler K, Zhutovsky S. Crack resistance and durability-related properties of internally cured high-strength/high-performance concrete. *Proceedings of 3rd International Conference on Durability of Concrete Structures*, Belfast, 17–19 September,1–9; 2012.
18. Reinhardt HW, Assmann A. Enhanced durability of concrete by superabsorbent polymers. In: *Brittle Matrix Composites 9*. Warsaw: Woodhead Publishing, 2009, 291–300.
19. Zhu J, Ma T, Fang Z. Characterization of agglomeration of reclaimed asphalt pavement for cold recycling. *Construct Build Mater* 2020b; **240**:117912. https://doi.org/10.1016/j.conbuildmat.2019.117912.
20. Craeye B, Geirnaert M, De Schutter G. Super absorbing polymers as an internal curing agent for mitigation of early-

age cracking of high-performance concrete bridge decks. *Construct Build Mater* 2011; **25**(1): 1–13.
21. Farzanian K, Teixeira KP, Rocha IP, et al. The mechanical strength, degree of hydration, and electrical resistivity of cement pastes modified with superabsorbent polymers. *Construct Build Mater* 2016; **109**:156–65.
22. Hu S, Zhou Y, Wang F, et al. Effect of super absorbent polymer particles on autogenous shrinkage and compressive strength of concrete. *J Huazhong Univ Sci Technol* 2008; **1**:1.
23. Pu X. *Super-High-Strength High Performance Concrete*. Boca Raton, Florida: CRC Press, 2012.
24. Tang F, Ma T, Zhang J, et al. Integrating three-dimensional road design and pavement structure analysis based on BIM. *Automat Construct* 2020a; **113**:103152. https://doi.org/10.1016/j.autcon.2020.103152.
25. Dang J, Zhao J, Du Z. Effect of superabsorbent polymer on the properties of concrete. *Polymers* 2017; **9**(12): 1–17.
26. Holt EE. Early age autogenous shrinkage of concrete. *VTT Publ* 2001; **446**:2–184.
27. Ma T, Wang H, Zhang D, et al. Heterogeneity effect of mechanical property on creep behavior of asphalt mixture based on micromechanical modeling and virtual creep test. *Mech Mater* 2017a; **104**:49–59.
28. Ding X, Ma T, Huang X. Discrete-element contour-filling modeling method for micromechanical and macromechanical analysis of aggregate skeleton of asphalt mixture. *J Transport Eng, Part B: Pavements* 2019b; **145**:1): 04018056. https://doi.org/10.1061/JPEODX.0000083.
29. Kim BJ, Yi C. Experimental study on the shrinkageproperties and cracking potential of high strength concrete containing industrial by-products for nuclear power plant concrete, *Nucl Eng Technol* 2017; **49**(1): 224–233.
30. Lura P, van Breugel K, Maruyama I. Effect of curing temperature and type of cement on early-age shrinkage of high-performance concrete. *Cem Concr Res* 2001; **31**(12): 1867–1872.
31. Zhu C, Li X, Wang B et al. Influence of internal curing on crack resistance and hydration of concrete. *J Build Mater* 2013; **16**(2): 221–225.
32. Zhang Y, Ma T, Ling M et al. Predicting dynamic shear modulus of asphalt mastics using discretized-element simulation and reinforcement mechanisms. *J Mater Civil Eng* 2019b; **31**(8): 04019163. https://doi.org/10.1061/(ASCE)MT.1943-5533.0002831.
33. Chen T, Luan Y, Ma T, et al. Mechanical and microstructural characteristics of different interfaces in cold recycled mixture containing cement and asphalt emulsion. *J Clean Prod* 2020; **258**:120674. https://doi.org/10.1016/j.jclepro.2020.120674.
34. Zhang Y, Ma T, Ding X, et al. Impacts of air-void structures on the rutting tests of asphalt concrete based on discretized emulation. *Construct Build Mater* 2018; **166**:334–44.
35. Ministry of Transport. *Test Methods of Materials Stabilized with Inorganic Binders for Highway Engineering (JTG E51–2009)*. Beijing: China Communications Press, 2009.
36. Tang F, Ma T, Guan Y, et al. Parametric modeling and structure verification of asphalt pavement based on BIM-ABAQUS. *Automat Construct* 2020b; **111**:103066. https://doi.org/10.1016/j.autcon.2019.103066.
37. Ding X, Chen L, Ma T, et al. Laboratory investigation of the recycled asphalt concrete with stable crumb rubber asphalt binder. *Construct Build Mater* 2019c; **203**:552–7.
38. Chen T, Ma T, Huang X, et al. The performance of hot-recycling asphalt binder containing crumb rubber modified asphalt based on physiochemical and rheological measurements. *Construct Build Mater* 2019; **226**:83–93.
39. Zhang Y, Ma T, Luo X, et al. Prediction of dynamic shear modulus of fine aggregate matrix using discrete element method and modified hirsch model. *Mech Mater* 2019c; **138**:103148. https://doi.org/10.1016/j.mechmat.2019.103148.
40. Ma T, Zhang D, Zhang Y, et al. Effect of air voids on the high-temperature creep behavior of asphalt mixture based on three-dimensional discrete element modeling. *Mater Design* 2015a; **89**:304–13.
41. Ma T, Huang X, Zhao Y, et al. Evaluation of the diffusion and distribution of the rejuvenator for hot asphalt recycling. *Construct Build Mater* 2015b; **98**:530–6.
42. Ma T, Wang H, He L et al. Property characterization of asphalt and mixtures modified by different crumb rubbers. *J Mater Civil Eng* 2017b; **29**(7): 04017036-1-10.
43. Ma T, Zhang D, Zhang Y et al. Simulation of wheel tracking test for asphalt mixture using discrete element modelling. *Road Mater Pavement Design* 2018; **19**(2): 367–384.